Angle-encoding Radiography

IU Neutron Group
(Dated: January 18, 2023)

We explore the possibility of neutron *angle-encoding radiography* (AER), a technique that allows the reconstruction of the transmission function of an arbitrary sample. The detector signal is shown to be the Fourier transform of the transmission function, which allows both qualitative (e.g. transmission function symmetry) and quantitative information of the sample's structure to be determined. This technique is sensitive to structures *smaller* than the usual geometric resolution R, which in this technique is an upper bound of the length scales of resolvable structures in traditional neutron transmission radiography.

I. INTRODUCTION

Neutron scattering techniques that employ *Larmor labeling* encode the path of a scattered neutron in the neutron's polarization. The Larmor phase Φ can be thought of classically as the change in angle of the neutron's polarization about the axis defined by the applied magnetic field. We are interested in the field integral of the magnetic Wollaston prisms (MWPs) because it is proportional to the Larmor phase of the neutron:

$$\Phi = \frac{\gamma_n m_n}{h}\lambda \int B\, d\ell = \frac{\gamma_n}{v_n}\mathrm{FI} = C_L \lambda \mathrm{FI} \tag{1}$$

where $\gamma_n = -1.832 \times 10^8$ rad s^{-1} T^{-1} is the gyromagnetic ratio of the neutron, m_n the mass of the neutron, h Planck's constant, λ the wavelength of the neutron, B the magnitude of the magnetic field integrated along the neutron's trajectory, and v_n the velocity of the neutron. We have also defined the field integral as FI$=\int B\, d\ell$ and the constant $C_L = \gamma_n m_n/h = -4.63 \times 10^{14}$ T/m^2. We note that FI $=$ FI(x, y, ϕ, ψ), but we will only consider FI $=$ FI(y, ϕ), i.e. we neglect the c and d aberration terms in the MWP field integral expansion in eq. (2).

Neutron transmission radiography is the technique of determining a sample's transmission function with contrast generated from the absorption and scattering of neutrons. AER can also determine the transmission function by Larmor labeling the path of the neutron through the material; doing so, we can resolve structures smaller than the geometric resolution $R = L_s D/L_d$ where L_s is the distance from sample to detector, D the diameter of the aperture, and L_d the distance from source to detector.

In both spin echo small angle neutron scattering (SESANS) and spin echo modulated small angle scattering (SEMSANS), the encoded pattern goes as the cosine of the Larmor phase. However, in SEMSANS the pattern is focused in position (only at the detector) while in SESANS, the pattern is focusing in angle. Both techniques require a *focusing condition*, a constraint among the magnetic fields that result in the largest aberration term(s) canceling, leaving a desired *encoding term*. In SESANS, this condition leaves a term proportional to horizontal divergence angle ϕ as the encoding term with a ϕ^2 aberration term which is effectively undetectable. We will show how this angle-encoding of the Larmor phase allows for the reconstruction of a sample's usual radiographic transmission function.

Throughout this analysis, we assume the beam is polarized in the $+y$ direction and analyzed in the $\pm y$ direction; we will refer to the parallel polarizer-analyzer configuration as the high count measurement and the antiparallel configuration as the low count measurement. We also do not take the effects of magnetic guide fields and other stray fields that will change the Larmor phase; we assume such contributions can be mostly compensated.

II. THE AER TECHNIQUE

In this section we explain the analytical basis of the technique, leaving the basic image reconstruction procedure to the next section. For the following calculations and McStas simulations, we use the following expansion for the field integral (FIE) of a single magnetic Wollaston prism [1]:

$$\mathrm{FI}(y, z, \phi, \psi) = ay + by\phi + cz\psi + dyz^2 \tag{2}$$

where ϕ the divergence angle of the neutron in the horizontal plane (x-y), ψ the divergence angle in the vertical plane (z-x), and a, b, c, d are experimentally determined parameters (see Fig. 1 for axes definitions). The expansion is taken about the geometric center of the prism, so the two divergence angles are defined relative to that same point; we also assume a paraxial beam, so we will use the small angle approximation through this analysis. Experimentally, we found that $a, b >> c, d$, so we neglect the smaller terms in this section (all are non-zero in the following numerical simulations).

Quantum mechanically, for a pure state, one can show the probability of an individual neutron detection in the high count setup (e.g. polarizer and analyzer axes parallel) to be

$$\langle P_{+y} \rangle = \cos^2\left[\frac{C_L}{2}\lambda \mathrm{FI}(y, \phi)\right] = \frac{1}{2}\left(1 + \cos\Phi\right). \tag{3}$$

where $P_{\pm y}$ are the spin-1/2 projection operators for the $|\pm y\rangle$ states. Implicit in this formula is perfect neutron initial polarization and analyzation; otherwise, we must

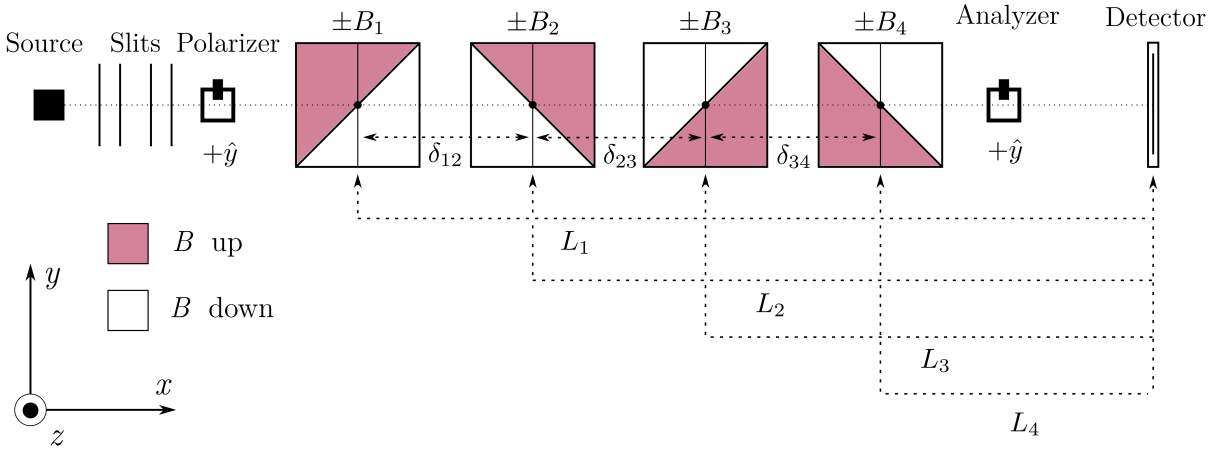

Figure 1.
Angle-encoding radiography experimental setup. The relevant focusing conditions are $B_1 = B_2$ and $B_3 = B_4$, and optionally with also $B_1 = B_3$ (called the SESANS focusing condition); the leading order aberration term goes as ϕ^2. We define δ_{ij} for $i, j \in \{1, 2, 3, 4\}$ as the center-to-center separation of the MWPs; for the existing generations of prisms, we note that the relative distances between prisms in the same vacuum chamber are immutable, so $\delta_{12} = \delta_{34} = \delta$.

consider the neutron state as a density matrix. Similarly, in the low count setup (e.g. polarizer and analyzer axes anti-parallel), we find

$$\langle P_{-y} \rangle = \sin^2 \left[\frac{C_L}{2} \lambda \mathrm{FI}(y, \phi) \right] = \frac{1}{2} \left(1 - \cos \Phi \right). \tag{4}$$

Therefore, we can calculate the neutron polarization P as

$$P = \frac{\langle P_{+y} \rangle - \langle P_{-y} \rangle}{\langle P_{+y} \rangle + \langle P_{-y} \rangle} = \cos \Phi. \tag{5}$$

Finally, we note that the detector signal $S(x_0, y_0)$ at some point (x_0, y_0) on the detector is proportional to $\langle P_{\pm y} \rangle$, and so after intensity normalization, $S \to I = \langle P_{\pm y} \rangle$ where I is the normalized detector intensity.

Next, we consider the master pixel equation (MPE):

$$I(\lambda, y, \phi) = \frac{1}{2} + \frac{\int d\lambda d\phi \, p_\lambda p_\phi \cos(C_L \lambda \mathrm{FI})}{2 \int d\lambda d\phi \, p_\lambda p_\phi} \tag{6}$$

where I is the normalized detector signal in the high count setup and p_λ and p_ϕ are the wavelength and horizontal divergence angle probability distributions, respectively [2]. The MPE states that the normalized detector signal at some point y away from the optical axis is an average over incoming neutron wavelengths and divergence angles. We neglect the masking effects of the MWPs, so we assume that the minimum (ϕ_1) and maximum (ϕ_2) divergence angles are simply

$$\phi_1 = \arctan \left(\frac{y - D/2}{L_d} \right) \tag{7}$$

$$\phi_2 = \arctan \left(\frac{y + D/2}{L_d} \right) \tag{8}$$

where D is the diameter of the source and L_d the distance from the source to the detector. As Φ is linear in λ, the wavelength integral in the MPE is simply the cosine Fourier transform of the wavelength probability distribution. If we assume a symmetric wavelength distribution (e.g. $p_\lambda = p_\lambda(\lambda - \overline{\lambda})$ where $\overline{\lambda}$ is the mean wavelength), we can further simplify the wavelength integral in the MPE:

$$\cos(C_L \overline{\lambda} \mathrm{FI}) \int d\lambda \, p_\lambda(\lambda) \cos(C_L \lambda \mathrm{FI}). \tag{9}$$

For a Gaussian [3] wavelength distribution with standard deviation $\delta\lambda$ and mean $\overline{\lambda}$, we have

$$p_\lambda = \exp \left[-\frac{(\lambda - \overline{\lambda})^2}{2 \, \delta\lambda^2} \right]. \tag{10}$$

We will assume a Gaussian wavelength distribution for the rest of this analysis. With this model, the master pixel equation becomes

$$I(y, \phi) = \frac{1}{2} + \frac{\int d\phi \, p_\phi e^{-\frac{1}{2}(C_L \delta\lambda \mathrm{FI})^2} \cos\left(C_L \overline{\lambda} \mathrm{FI}\right)}{2 \int d\phi \, p_\phi}. \tag{11}$$

Notice that we obtain the expected single neutron probability when $\delta\lambda \to 0$ shown in eq. (3), and that the finite wavelength spread causes the fringes to die exponentially away from the echo condition ($\Phi = 0$). We will also see that the data analysis becomes more difficult as the signals I are no longer completely orthogonal, but have a small overlap that must be tracked.

We now derive the focusing condition necessary for pure angle-encoding and show that the conventional SESANS setup (i.e. all prism hypotenuses orientated in the same sense) is less general than the LISANS [4] setup in which the second and fourth prisms have their

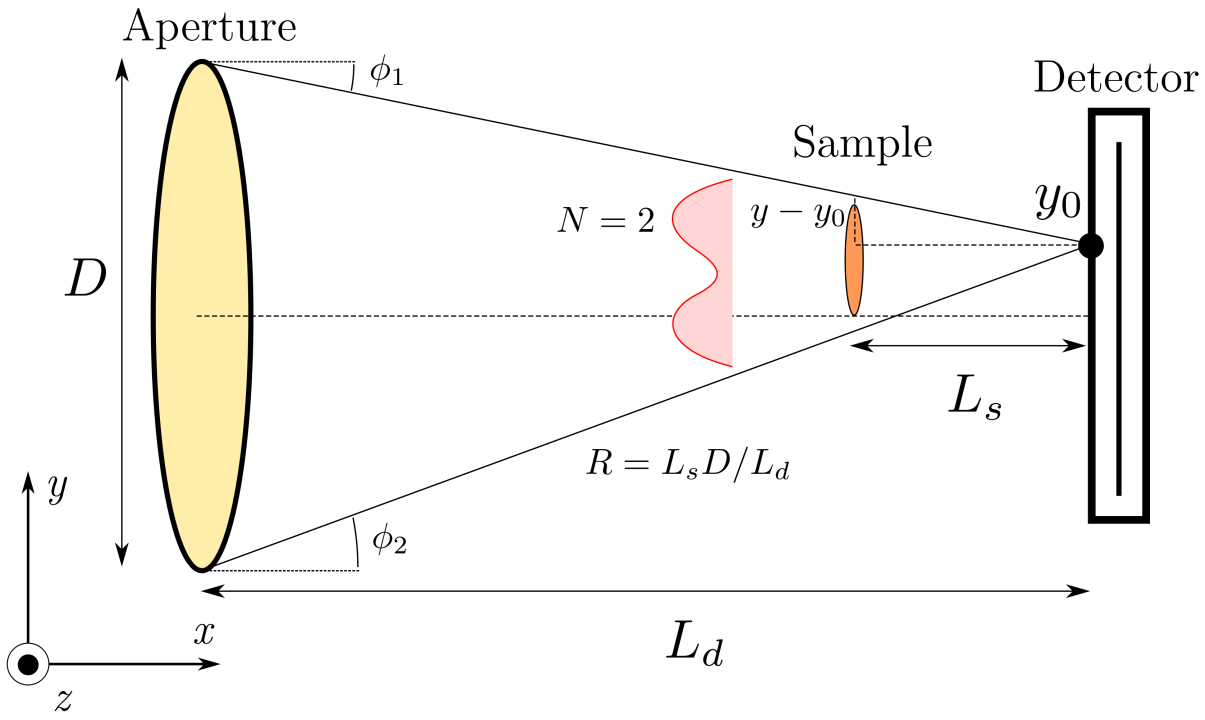

Figure 2.
Definition of essential beamline parameters where D is diameter of the aperture which is a distance L_d from the detector while the sample is a distance L_s away from the detector. The structure of interest (orange oval) must be smaller than the geometric resolution R to be visible with this technique. The perspective of the pixel y_0 is also shown to be determined by the maximum and minimum angles ϕ_2 and ϕ_1, respectively.

hypotenuses in the reverse sense (see fig. 1). For traditional (unfocused) SESANS, the field integral experienced by a neutron impinging on the detector a distance y_0 from the center becomes

$$\mathrm{FI}(y_0, \phi) = (a + b\phi)\left[(B_1 - B_2 + B_3 - B_4)y + (B_4 L_4 - B_3 L_3 + B_2 L_2 - B_1 L_1)\phi\right] \tag{12}$$

where B_i are the magnetic fields in each triangular field region and L_i are the distances from the MWP centers to detector for $i \in \{1, 2, 3, 4\}$, as shown in fig. 1. In SESANS focusing, used in the technique of the same name, we would like to cancel the entire field integral over the detector, but we lack the necessary degrees of freedom to do so. Thus only the leading order y is canceled and the ϕ term remains when applying the focusing condition of all fields having an equal magnitude of B:

$$\mathrm{FI}(y_0, \phi) = (a + b\phi)B(L_4 - L_3 + L_2 - L_1)\phi. \tag{13}$$

The distance between the prisms in each vacuum chamber is fixed at δ (see fig. 1), so the field integral reduces to

$$\mathrm{FI}(y_0, \phi) = -2\delta B(a + b\phi)\phi. \tag{14}$$

Later, we will show how this previously unwanted remaining ϕ term in the field integral becomes the crux of AER. However, this field integral is not suitable for the general AER technique as δ is fixed by the design of the prisms. To solve this issue, we must invert the hypotenuses of the second and fourth triangular field regions; doing so, we obtain

$$\begin{aligned}\mathrm{FI}(y_0, \phi) &= (L_4 - L_2 + L_3 - L_1)B(a + b\phi)\phi \\ &= -2(\delta + \delta_{23})B(a + b\phi)\phi\end{aligned} \tag{15}$$

where δ_{23} is the distance between the centers of the second and third prisms, which is an easily adjustable experimental parameter. From this point on, we neglect the higher term as $\phi^2 \approx (y/L_d)^2 \ll \phi$.

The focusing used in eq. (15) is a simple but potentially restrictive method to generate pure angle encoding; alternatively, the most general focusing condition requires that $B_1 + B_2 = B_3 + B_4$ and $B_1 - B_2 = B_3 - B_4$.

Using this condition, we find

$$\begin{aligned}\mathrm{FI}(y_0,\phi) =& B_1(L_3-L_1)(a+b\phi)\phi \\ &+ B_2(L_4-L_2)(a-b\phi)\phi \\ \approx& \left[B_1(L_3-L_1)+B_2(L_4-L_2)\right]a\phi \\ =& -(\delta+\delta_{23})(B_1+B_2)a\phi\end{aligned} \tag{16}$$

when we ignore the small ϕ^2 term. Therefore, we have generated pure angle encoding can probe sub-resolution structures.

We now explicitly include the transmission function T in our analysis. For clarity, we will assume $\delta\lambda = 0$ for the following derivation, but restore it when discussing how to process the intensity data. In the high count setup, the normalized signal at some point y_0 on the detector is

$$\begin{aligned}I(y_0) &= \frac{1}{2}\int_{\phi_1}^{\phi_2} d\phi\, T\,(1+\cos k\phi) \\ &= \frac{1}{2L_s}\int_{y_0-R/2}^{y_0+R/2} dy\, T(y)\left[1+\cos\frac{k}{L_s}(y-y_0)\right]\end{aligned} \tag{17}$$

where $T(y)$ is the transmission function at the point y of the sample and we take the frequency (in horizontal divergence angle) to be

$$k = C_L\overline{\lambda}a\left[B_1(L_3-L_1)+B_2(L_4-L_2)\right]. \tag{18}$$

Notice the appearance of the geometric resolution $R = L_sD/L_d$ in the limits of the integral; therefore the resolution is the *largest* length scale at which this technique can probe the sample. As we have complete experimental control over the frequency k, we can choose it to have a period some multiple of the resolution; in other words, choose $k = 2\pi nL_s/R$ for $n \in \mathbb{N}^+$. In this way, the detector signal will will be the Fourier transform of the transmission function of the sample, with the fundamental frequency being $2\pi/R$. Plugging this choice of k in, we see

$$I_n(y_0) = I_0 + \frac{1}{2L_s}\int_{y_0-R/2}^{y_0+R/2} dy\, T(y)\cos\frac{2\pi n}{R}(y-y_0) \tag{19}$$

where we define $I_0 = \frac{1}{2L_s}\int_{y_0-R/2}^{y_0+R/2} dy\, T(y)$. All that remains is to describe how to obtain said information about the transmission function.

As a final note, in the usual SESANS focusing, we take $B_1 = B_2$, so then all field magnitudes are equal to

$$B = \frac{2\pi nL_s}{R}\frac{1}{C_L\overline{\lambda}a(L_4+L_3-L_2-L_1)}. \tag{20}$$

However, that additional restriction is not necessary to obtain pure angle encoding. An alternate focusing condition would be to fix one of the magnetic fields; without loss of generalization, we choose B_1 to be some free value. Then, we must have

$$B_2 = \frac{\frac{2\pi nL_s}{R}\frac{1}{C_L\overline{\lambda}a} - B_1(L_3-L_1)}{L_4-L_2} \tag{21}$$

for proper angle encoding.

III. IMAGE RECONSTRUCTION

Now we walk through the image reconstruction algorithm for both the idealized $\delta\lambda = 0$ case as well as the $\delta\lambda > 0$ case. We see the integral inversion becomes more difficult with the addition of a finite wavelength spread as the functions are no longer orthogonal, but are still almost orthogonal. In both derivations, we will write the transmission function as a Fourier series:

$$\begin{aligned}T(y) =& \frac{a_0}{2} + \sum_{n>0} A_n\cos\left(\frac{2\pi n}{R}(y-y_0)\right) \\ =& \frac{a_0}{2} + \sum a_n(y_0)\cos\left(\frac{2\pi n}{R}y\right) \\ &+ \sum b_n(y_0)\sin\left(\frac{2\pi n}{R}y\right)\end{aligned} \tag{22}$$

where the cosine and sine Fourier coefficients are

$$a_n(y_0) = A_n\cos\left(\frac{2\pi n}{R}y_0\right) \tag{23}$$

$$b_n(y_0) = A_n\sin\left(\frac{2\pi n}{R}y_0\right). \tag{24}$$

Different points y_0 on the detector will give different linear combinations of Fourier components. Therefore a two dimensional detector is required for complete sample characterisation, as the center $y_0 = 0$ only gives the cosine components.

A. No wavelength spread

Here we suppose that $p_\lambda = \delta(\lambda - \overline{\lambda})$, so eq. (19) is exact. Plugging in eq. (22) into eq. (19) and using orthogonality, we find

$$a_0 = \frac{2L_s}{R}I_0 \tag{25}$$

$$a_n = \frac{4L_s}{R}I_n(y_0^c) - a_0 \tag{26}$$

$$b_n = \frac{4L_s}{R}I_n(y_0^s) - a_0 \tag{27}$$

where we have selected the points $y_0^c = Rm/n$ and $y_0^s = R(4m+1)/4n$ for $m \in \mathbb{N}$ as to give purely a_n and b_n, respectively. From these equations, we see that to distinguish between the cosine and sine Fourier coefficients near $y_0 = 0$, we would need a detector with pixel size p to be $p < R/4n$. This constraint is only a rough estimate on the maximum pixel size; in a real experiment with $p \approx R$, the detector signal will be an average of a linear combination of Fourier coefficients.

B. Gaussian wavelength spread

For the $\delta\lambda \neq 0$ case, the presence of the Gaussian prevents the use of orthogonality when inverting the integral

equation to find $T(y)$. However, we will show that the overlaps are small enough to be ignored for reasonable choices of $\delta\lambda$ for the fundamental and lower harmonics. We start with eq. (19) and insert the Gaussian factor [5], which we then invert using the same Fourier expansion for $T(y)$ that we used in the zero wavelength spread case. The family of integrals S_{nm} we need to calculate is therefore of the form

$$\begin{aligned} S_{nm} &= \int_{y_0-R/2}^{y_0+R/2} dy\, e^{-\frac{1}{2}\left(\frac{2\pi n}{R}(y-y_0)\lambda_f\right)^2} \cos\frac{2\pi n}{R}(y-y_0)\cos\frac{2\pi m}{R}(y-y_0) \\ &= \frac{R}{2\sqrt{2\pi}n\lambda_f}\sum_{\{\pm\}}\exp\left(-\frac{(m\pm n)^2}{n^2\lambda_f^2}\right)\mathfrak{Re}\mathrm{Erf}\left(\frac{n\pi}{\sqrt{2}\,\lambda_f}+\frac{i(m\pm n)\lambda_f}{\sqrt{2}n}\right) \end{aligned} \tag{28}$$

where $m, n \in \mathbb{N}$, $\mathfrak{Re}\mathrm{Erf}(\cdot)$ denotes the real part of the error function of a complex argument, and $\lambda_f = \delta\lambda/\overline{\lambda}$ is the fractional wavelength spread. The Fourier coefficients are

$$a_0 = \frac{4L_s}{R}S_{00} = \frac{4L_s}{R}I_0 \tag{29}$$

$$A_m = \frac{2L_s I_n(y_0) - \frac{a_0}{2}(R - S_{n0}) - \sum' A_{m'}S_{nm'}}{S_{nm}} \tag{30}$$

where the prime on the sum of m' denotes the constraints $m' \neq m$ and $m' > 0$. Note that we can still use equations (23) and (24) to find a_m and b_m from A_m, respectively. Although the sum over m' is infinite, the Fourier coefficients are still finite. Using the well-known dirac delta function identity

$$\delta\left(\frac{2\pi}{R}(y-y_0)\right) = \frac{1}{2\pi}\sum_{m=-\infty}^{\infty} e^{im\frac{2\pi}{R}(y-y_0)} \tag{31}$$

we see that when including the $m' = 0$ term in the sum, then $\sum_{m'} S_{nm'} = R/2$ for any choice of $\delta\lambda \geq 0$. Assuming the transmission function has a converging Fourier series (e.g. has bounded variation), an application of the Cauchy-Schwartz inequality shows the overall sum is finite.

Unfortunately, we are left with a linear combination of Fourier components due to the Gaussian factor. However, if we assume that $\delta\lambda < 10\%$, we can still extract at least the first 10 harmonics, with the upper limit of obtainable harmonic depending on how quickly the Fourier series of the transmission function $T(y)$ converges. Table I shows how badly orthogonality breaks down when $\delta\lambda = 10\%$, with all values being rounded to the nearest 10^{-3}, for clarity. However, when $\delta\lambda = 1\%$, the integrals S_{nm} are zero for $n \neq m$ until $n = 33$ when rounded to the nearest thousandth, with the non-zero values decreasing steadily and monotonically from $R/2$ to $R/2 \times 0.846$. As expected, the number of extractable Fourier coefficients depends heavily on the wavelength spread as well as exact knowledge of the wavelength distribution of the beam.

The error grows with n due to the loss of orthogonality and due to the eventual truncation of the sum due to finite experimental data. Eventually for some (large) harmonic, we must guess the coefficient, which will introduce a small error in the smaller harmonics due to the infinite sum in (30). However, as shown in Tab. I, we expect that error to be small for $n < 10$ even when the wavelength spread is as large as ten percent. To extract the coefficients we diagonalize the matrix containing the values of S_{nm}, with the eigenvalues being the desired Fourier coefficients of the transmission function.

IV. ANALYTIC CALCULATION OF SOME TRANSMISSION FUNCTIONS

Here we derive the analytic expression for the two-slit transmission function that is simulated in sec. V as well as a more general form suitable for any one dimensional sample.

A. Two-slit Transmission Function

Assuming the transmission function is unity at the openings of the slits and zero everywhere else, the transmission function becomes

$$\begin{aligned} T(y) =& \Theta\left(y+\frac{3q}{2}\right)\Theta\left(-\frac{q}{2}-y\right) \\ &+ \Theta\left(y-\frac{q}{2}\right)\Theta\left(\frac{3q}{2}-y\right) \end{aligned} \tag{32}$$

where $\Theta(x)$ is the Heaviside step function and q is the width of the opening and the distance between the interior edges of the two slits; this function is the sum of two rectangle functions (also called boxcar functions [6]). We have assumed that the center of the double slit pattern is on the optical axis. As an aside, we need $|y_0 \pm R/2| \gg 3q$ to obtain a quickly converging series. Direct computation of the integral in the $\delta\lambda = 0$ limit yields

$$I_n(y_0) = \frac{q}{L_s} + \frac{R}{\pi n L_s}\sin\left(\frac{\pi n}{R}q\right)\cos\left(\frac{2\pi n}{R}q\right)\cos\left(\frac{2\pi n}{R}y_0\right). \tag{33}$$

Note that the double slit generates a Moire pattern at the detector with a period of R/n. As this transmission

Table I. Table of the values of the integral S_{nm}/R with $\lambda_f = \delta\lambda/\overline{\lambda} = 10\%$ for $m \in \{0, 1, \ldots, 9\}$ and $n \in \{1, 2, \ldots, 8\}$ rounded to the nearest 10^{-3} for clarity (row index n and column index m). For the case $\lambda_f = 0$, this table would reduce to $\delta_{nm}/2$ by orthogonality.

	0	1	2	3	4	5	6	7	8	9
1	0.005	0.491	0.001	0	0	0	0	0	0	0
2	-0.004	0.002	0.468	0.001	0	0	0	0	0	0
3	0.003	-0.002	0.001	0.434	0.001	0	0	0	0	0
4	-0.002	0.001	-0.001	0.003	0.394	0.003	0	0	0	0
5	0.001	-0.001	0.001	-0.001	0.011	0.352	0.011	0	0	0
6	-0.001	0.001	0	0	0	0.024	0.312	0.024	0	0
7	0	0	0	0	0	0	0.039	0.277	0.039	0
8	0	0	0	0	0	0	0	0.054	0.246	0.053

function is even, all sine Fourier components b_n are zero; thus, we must see oscillations at the detector as we must have $I_n(y_0^s) = 0$ for all y_0^s and $I_n(y_0^c) \neq 0$ for all y_0^c (some cosine coefficients will be zero due to selection rules from this choice of T). For a finite wavelength spread, eq. (33) would qualitatively describe the detector intensity, but the oscillations would dampen as y_0 increases.

B. General Transmission Function

Here we generalize the result of the previous section by considering a piecewise constant transmission function of arbitrary partition size δy. The natural choice for such a partition is the detector's pixel size. The transmission T_p for each pixel p can also be a complex number, which, for example, could represent a birefringent sample. The analytic form for such a function is

$$T(y) = \sum_p T_p \Theta\left(y - \frac{R}{2} + (p-1)\delta y\right) \Theta\left(-\frac{R}{2} + p\delta y - y\right) \tag{34}$$

where each T_p is some complex number with $0 \leq |T_p| \leq 1$ and δy the partition size. The sum goes over all pixels in the detector. Direct computation of the integral in the $\delta\lambda = 0$ limit yields

$$\begin{aligned} I(y_0) =& I_0 + \frac{R}{4\pi n L_s} \sum_p T_p \left(\sin\left[\frac{2\pi n}{R}\left(-\frac{R}{2} + p\delta y - y_0\right)\right] - \sin\left[\frac{2\pi n}{R}\left(-\frac{R}{2} + (p-1)\delta y - y_0\right)\right]\right) \\ =& I_0 + \frac{R}{2\pi n L_s} \sum_p T_p \sin\left(\frac{2\pi n}{R}\frac{\delta y}{2}\right) \cos\left[\frac{2\pi n}{R}\left(-\frac{R}{2} + \delta y \frac{2p-1}{2} - y_0\right)\right] \end{aligned} \tag{35}$$

where we define $I_0 = \delta y/(2d) \sum_p T_p$.

V. TO DO: MCSTAS SIMULATIONS

Here we give a few examples of image reconstruction using AER with McStas simulations. Table II shows the beamline parameters used; SESANS focusing was used, so all MWP currents were equal.

VI. OUTLOOK

- Need a high resolution detector otherwise pixels will mix Fourier components
- Wavelength spread not an issue up to 10%
- Sub-geometric resolution resolving capability
- Get global information of the transmission function

[1] F. Li, S. R. Parnell, W. A. Hamilton, B. B. Maranville, T. Wang, R. Semerad, D. V. Baxter, J. T. Cremer, and R. Pynn, Rev. Sci. Instr. **85**, 053303 (2014).

Table II. Simulation parameters for each harmonic n. MWP magnetic field B, neutron wavelength $\overline{\lambda} \pm \delta\lambda$, distances of components relative to the detector L, and source diameter D are listed below. The resolution R is given by $R = L_s D/L_d = 2.4$ mm.

$\overline{\lambda} \pm \delta\lambda$ (Å)	B (mT)	L_1 (m)	L_2 (m)	L_3 (m)	L_4 (m)	L_d (m)	L_s (m)	D (mm)
$2.0 \pm 5\%$	$-0.367n$	4	3	2	1	5	1	10

[2] Because the ψ dependent terms are so small, we can take $p_\psi = \delta(\psi)$.

[3] For the less realistic uniform distribution $p_\lambda = 1$ for $\lambda \in [\overline{\lambda} - \delta\lambda, \overline{\lambda} + \delta\lambda]$, the exponential is replaced by $\mathrm{sinc}(C_L \delta\lambda \mathrm{FI})$.

[4] Linearly improved (SEM)SANS.

[5] Insertion of sinc instead will result in a similar expression with $\mathfrak{Re}\mathrm{Erf}(\cdot)$ replaced by a sum of four sine integrals $\mathrm{Si}(\cdot)$ with arguments $\pi[m + n(\lambda_f - 1)]$, $\pi[m - n - n\lambda_f]$, and $\pi[m + n \pm n\lambda_f]$ with an overall constant of $R/(4n\pi\lambda_f)$.

[6] A mathematically equivalent definition for the transmission is $T(y) = \Theta(y + 3q/2) - \Theta(y + q/2) + \Theta(y - q/2) - \Theta(y - 3q/2)$.